Decomposition of hypo-eutectoid Fe-C austenites; a numerical diffusion model

V. M. Mesnan Silalahi, Marcel Onink and Sybrand van der Zwaag

A numerical model is presented which describes the growth rate of ferrite during the decomposition of austenite in Fe-C alloys. The growth rate is modelled assuming carbon diffusion in austenite as the rate determining mechanism. The effect of the definition of the diffusion coefficient of carbon in austenite on the growth rate is shown. The model is used to examine the effects of initial carbon concentration, the local carbon concentration in austenite at the interface and the initial austenite grain size on the growth rate. Good agreement between theoretical results and both new and existing experimental data was observed.

Numerisches Diffusionsmodell zum untereutektoidischen Austenitzerfall. Ein numerisches Modell beschreibt die Ferritwachstumsgeschwindigkeit während des Austenitzerfalls in Fe-C-Legierungen. Die Wachstumsgeschwindigkeit wird unter der Voraussetzung, daß die Kohlenstoffdiffusion im Austenit der geschwindigkeitsbestimmende Mechanismus ist, modelliert. Mit dem Modell wird die Wirkung der Kohlenstoffanfangskonzentration, der örtlichen Kohlenstoffkonzentration im Austenit an der Grenzfläche und der anfänglichen Austenitkorngröße auf die Wachstumsgeschwindigkeit ermittelt. Zwischen den theoretischen Ergebnissen und Versuchswerten, sowohl neuen als auch bestehenden Daten, herrscht gute Übereinstimmung.

The transformation from austenite to ferrite in Fe-C alloys and commercial steels has been studied in great detail because of its technological importance in steel production and heat treatments. Models describing the kinetics of the transformation can be separated into different groups. Some models describe the transformation process as a whole commonly using the Johnson-Mehl-Avrami-equation [1...7]. The parameters resulting from this equation are only applicable to a group of steels exhibiting a comparable transformation behaviour and can only be used for a numerical description instead of the prediction of the kinetics of the transformation.

The predictive power of the calculations can be enhanced by employing physical models describing the active mechanisms in the transformation. In the case of the austenite to ferrite transformation these involve nucleation and growth. However, the modelling of nucleation processes in solid-solid transformations is still mainly phenomenological. For moderate undercoolings nucleation often takes place at the austenite-grain boundaries. Thus, to be able to understand the nucleation process, knowledge on the grain-boundary structure and grain-boundary distributions is indispensable. However, very few experiments have been devoted to the determination of these parameters [8].

Growth, on the other hand, depends primarily on the atomic mobility of the iron and carbon atoms. The transformation from austenite to ferrite involves reconstructive diffusion of the iron atoms at the transformation interface and long-range diffusion of carbon in austenite; as a result diffusion based growth models are commonly used for the calculation of the transformation kinetics. To incorporate nucleation effects specific assumptions are made such as site-saturation [9], which effectively corresponds to neglecting nucleation [10...12]. The concept of a fixed incubation time before the ferrite nucleates has also been proposed [11; 13]. Results shown in [10] for Fe-0.5 % C (compositions are always expressed as mole fractions in %) show a satisfactory agreement for the calculated and experimental nucleation period but application of the same model to Fe-C-Mn steels shows highly unacceptable differences.

Ir. V. M. Mesnan Silalahi; Dr. Marcel Onink, (now with Applied Physical Metallurgy-Hot Rolled Products, Corporate Research Laboratory, Hoogovens Groep BV, IJmuiden); *Professor Dr. Ir. Sybrand van der Zwaag*, Heat Treatment Technology, Laboratory for Materials Science, Delft University of Technology, Delft, The Netherlands.

In this work, the kinetics of the decomposition of austenite into ferrite in Fe-C alloys is described assuming instantaneous nucleation of ferrite everywhere along the austenite-grain boundary and diffusion of carbon in austenite as the rate-determining step in the growth process. Fick's second law of diffusion is solved by applying a finite difference model for spherical austenite grains. In contrast to previous work local equilibrium is not maintained continuously at the transformation interface. Instead, the carbon concentration in austenite at the interface is allowed to change. The dependence of the diffusion coefficient of carbon in austenite on the carbon concentration is taken into account. The influence of grain size, initial average carbon concentration and the carbon concentration in austenite at the interface on the kinetics of the decomposition is investigated. Experimental verification of the numerical model is achieved using quantitative metallography to determine the fraction of ferrite and the austenite grain size in the microstructures obtained after partial isothermal transformation of an Fe-0.8 % C alloy at 973 K. Carbon concentrations near the interface were determined using electron-probe microanalysis. Comparison of the present calculations to literature data for the growth rate of allotriomorphic ferrite in the same temperature region [14] showed an excellent agreement.

Model description

The present model is restricted to the decomposition of austenite into pro-eutectoid ferrite. The ferrite is considered to nucleate along the austenite-grain boundary and growth takes place towards the centre of the austenite grain. The austenite grain is assumed to be spherical. Because the calculations presented in this work are compared to experiments with relatively high undercooling, the concept of site-saturation can be applied, as was supported by the observed microstructures using light microscopy (see below). For a single austenite grain the decomposition is modelled assuming symmetrical growth of ferrite.

The observed microstructure can be translated into a linear mesh as shown in **figure 1**. Each cell in the mesh represents the carbon concentration at a certain position in the austenite grain at a certain time. By adopting symmetrical growth of the ferrite only half of the grain has to be incorporated in the calculations. Due to the finite dimensions of the austenite grain overlap of diffusion fields from ferrite

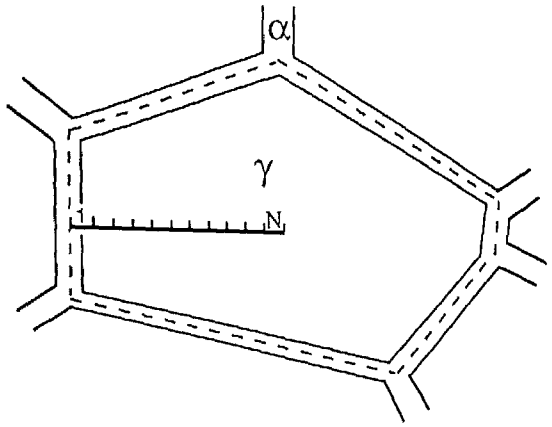

Figure 1. Schematic representation of the microstructure during the initial stages of the decomposition of austenite into ferrite. The mesh shows the translation of the two-dimensional structure into the single space variable used for the calculation. The dashed line indicates the former austenite grain boundary

layers growing from opposite directions eventually leads to an increase in the carbon concentration at the centre of the grain. Conservation of mass is preserved by treating the centre of the austenite grain as a point of no mass transfer.

The diffusion of carbon in the austenite grain can be approximated by calculating the flux in each cell. For a constant diffusion coefficient of carbon in austenite this flux is given by (for list of symbols, see **table 1**):

$$\frac{\partial c^\gamma}{\partial t} = \frac{1}{r^2}\frac{\partial}{\partial r}\left(r^2 D_C^\gamma \frac{\partial c^\gamma}{\partial r}\right). \tag{1}$$

Analytical solutions to the diffusion equation with the diffusion coefficient dependent on the local composition do not exist for finite media. Therefore, in the calculation of the transformation kinetics an average diffusion coefficient has to be used or the diffusion equation has to be solved numerically.

Table 1. List of symbols

[A]	diffusion matrix
c^0	initial carbon concentration
$c^\gamma(r,t)$	carbon concentration profile along the radius
$c^{\gamma/\alpha}$	carbon concentration in austenite at the interface
c_c^γ	carbon concentration in austenite in the centre of the grain
c^α	carbon concentration in ferrite
$c^{\alpha/\gamma}$	carbon concentration in ferrite at the interface
c_t	carbon concentration profile in austenite at time t
$c_{t+\Delta t}$	carbon concentration profile in austenite at time $t+\Delta t$
D_C^γ	concentration dependent diffusion coefficient of carbon in austenite
D_1	concentration dependent diffusion coefficient
D_2	position averaged diffusion coefficient
D_3	concentration averaged diffusion coefficient
ξ	location of the interface
x	atom fraction of carbon in austenite
r	position along the radius of the grain
Δr	size step in calculation
R	grain radius
s	meshparameter, $\Delta t/\Delta r^2$
t	transformation time
Δt	time-step
T	temperature
y_C	site fraction of carbon in austenite at the interstitial lattice
Ω	supersaturation

To approximate equation (1) numerically, an implicit method was applied [15]. Applying this equation to each point of the mesh in figure 1 leads to the formation of an $N \times N$ matrix [A]. The matrix equation is defined as:

$$\begin{aligned} &-D_i s \cdot c_{i-1}^\gamma\,(t+\Delta t)\cdot\frac{r_{i-1}}{r_i} \\ &+\,(1+2D_i s)\cdot c_i^\gamma\,(t+\Delta t) \\ &-D_i s \cdot c_{i+1}^\gamma\,(t+\Delta t)\cdot\frac{r_{i+1}}{r_i} = c_i^\gamma(t). \end{aligned} \tag{2}$$

Effectively, the matrix is inverted and applied to the profile calculated in the previous cycle:

$$[\mathrm{A}]\cdot c_{t+\Delta t} = c_t \Rightarrow c_{t+\Delta t} = [\mathrm{A}]^{-1}\cdot c_t. \tag{3}$$

The starting condition at $t = 0$ used in the calculation is:

$$r = 0 \qquad c = c^{\gamma/\alpha},$$

$$r > 0 \qquad c = c^\gamma.$$

During the calculation the atom balance of the total number of carbon atoms dictates the boundary movement. As the transformation interface proceeds, the main elements of [A] which are 'located' in the ferrite are set equal to one and off-row elements are set to zero, thereby keeping the carbon concentration in ferrite constant. Mostly, the diffusion equations at the transformation interface are solved under the assumption of thermodynamic equilibrium at the interface [9...13; 16]. The carbon concentrations at the interface in austenite and in ferrite equal the equilibrium concentrations as given by the phase diagram and thus the differences in chemical potential of Fe and C across the interface are nil. Maintaining this equilibrium value at the interface during a time-step in the calculation numerically provides an overshoot of carbon in the austenite. This overshoot of carbon in the austenite is then balanced by a movement of the interface, enlarging the amount of ferrite. This approach is known as the quasi-stationary approach, or the in-variant size approximation. The diffusion equation is solved for an immobile interface, and the location of the interface is subsequently determined by applying a mass balance across the interface:

$$\int_0^\xi (c^0 - c^\alpha)4\pi r^2 \mathrm{d}r = \int_\xi^R (c^\gamma(r;t) - c^0)4\pi r^2 \mathrm{d}r. \tag{4}$$

In this approach it is assumed that the progress of the transformation is solely determined by the gradient of the carbon concentration in austenite and the role of the transformation interface itself is effectively ignored. If local equilibrium is not imposed at the interface when the interface stands still, the carbon just redistributes in the austenite and the carbon concentration in austenite at the interface is reduced. Such redistribution will not lead to a displacement of the interface since no 'extra' carbon is added to the austenite. The transformation is now said to proceed in a more interface controlled mode. In the present work, the following procedure was applied to calculate the growth of ferrite. In the first time step of the calculation the carbon concentration in austenite at the interface is put at the local equilibrium

value. Then, the carbon redistribution during the next time step is calculated. This leads to a reduction of the carbon concentration at the interface. The carbon concentration at the cell corresponding to the interface is then increased by half the difference between the current concentration and the local equilibrium concentration and the new carbon concentration profile is calculated in the next calculation cycle. This procedure is repeated until the total amount of carbon added can be balanced by advancing the ferrite interface one mesh distance. The procedure followed resembles the conditions for mixed mode transformations, where local equilibrium does not exist at all times. A justification for this approach is given in the discussion. An example of the variation of the local carbon concentration at the interface during the transformation is shown in **figure 2.**

Essential in a (numerical) diffusion model is the appropriate definition of the diffusion coefficient. In the case of austenite decomposition the relevant diffusion coefficient is that of carbon in austenite. As the diffusion coefficient of carbon in austenite is a strong function of the carbon concentration [17]:

$$D_1 = D_C^\gamma = 4.53 \cdot 10^{-7} \left(1 + y_C(1-y_C)\frac{8339.9}{T}\right) \cdot \quad (5)$$

$$\exp\left\{-\left(\frac{1}{T} - 2.221 \cdot 10^{-4}\right)(17767 - y_C \cdot 26436)\right\} \text{ m}^2\text{s}^{-1}$$

proper incorporation of this effect on the interface velocity is by no means trivial. In the present work three different approaches are compared. In the first approach each cell in the mesh has the diffusion coefficient appropriate to the carbon concentration of that cell, D_1, which is the most correct approach. The diffusion equation is solved in the separate cells, the calculations are performed using a concentration dependent diffusion coefficient. This approach has also been followed in recent studies on the growth of ferrite allotriomorphs [11] and growth of ferrite from austenite grain boundaries [13].

Alternatively, a constant diffusion coefficient can be used. This constant diffusion coefficient can be defined in several ways. In [9] the effective diffusion coefficient was calculated by averaging over the entire remaining austenite grain. This is procedure D_2:

$$D_2 = \frac{\int_\xi^R D_C^\gamma(c(r))\mathrm{d}r}{R-\xi} \cdot \quad (6)$$

The value for the diffusion coefficient increases with progressing transformation.

Since the diffusion of the solute takes place near the interface, instead of considering the entire austenite grain, one can restrict the area of interest to the diffusion zone just ahead of the interface. In such a simplification the effective diffusion coefficient D_3 can be calculated by averaging over the possible concentrations in the diffusion zone:

$$D_3 = \frac{\int_{c_0^\gamma}^{c^{\gamma/\alpha}} D_C^\gamma(c)\mathrm{d}c}{c^{\gamma/\alpha} - c_{\min}} \cdot \quad (7)$$

This diffusion coefficient underestimates the true diffusion coefficient near the interface, and somewhat overestimates the diffusion coefficient at the end of the diffusion zone.

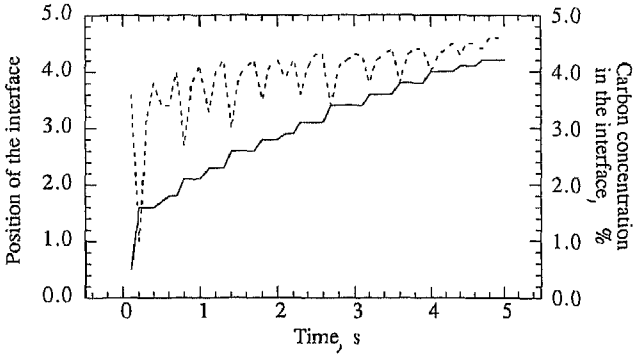

Figure 2. Variation of the interface concentration with transformation time, calculated for an Fe 0.8 % C alloy isothermally transformed at 973 K during 5 s with a grain diameter of 25 μm. The solid line represents the movement of the interface, the dashed line represents the carbon concentration at the interface

Overlapping diffusion fields (soft-impingement) increases the value of $c_{\min}$ and thus the value of D_3 [10]. In the results to be described the effect of the definition of the diffusion coefficient is described.

The convergence and stability of all calculations was ascertained by choosing Δt and Δx such that the ratio $D\Delta t/\Delta x^2 < 1$.

Experimental

Dilatometry. To ensure a well-defined thermal history specimens from a high purity Fe-0.8 % C alloy (0.0007 % Mn; 0.001 % Cr; 0.005 % Cu; 0.0003 % Mo; 0.0004 % Ni, 0.005 % Sn; balance Fe) investigated were given an appropriate heating cycle in a dilatometer. The thermal treatment consisted of an austenitising step (1373 or 1273 K for 10 min), quenching to the transformation temperature in the ferrite/cementite two-phase region, i.e. 973 or 923 K, isothermal anneal at the transformation temperature, followed by quenching to room temperature. Both fully transformed and partially transformed samples were prepared. The tubular specimens had a length of 10 mm, an outer diameter of 3 mm, and a wall thickness of 0.25 mm. The cooling rate during quenching with Helium gas was approximately 200 K $\cdot$ s^{-1}. The temperature was measured with a Pt/Pt-10 % Rh thermocouple, which was spot-welded to the specimen. Heating of the specimen in a vacuum of 3 $\times$ 10^{-3} Pa occurred by inductive heating using a high frequency generator (for further details of measurement and evaluation see [18]).

Visible light microscopy. Visible light microscopy was performed using a microscope equipped with a 100 $\times$ 0.95 objective corrected for oil immersion. After grinding and final polishing with 1 μm diamond paste the samples were etched for 10 s with a 1 % Nital (HNO_3 in ethanol) solution. Subsequently, these samples were physically etched by deposition of a $\lambda/4$ layer ZnTe for 550 nm monochromatic illumination. In this way, the contrast between the ferrite phase and martensitic phase is strongly enhanced. The quantative image analyser is connected to a microscope equipped with planochromat 20 $\times$ 0.40 and 50 $\times$ 0.80 objectives and a 500 $\times$ 582 pixels colour CCD camera.

Electron probe microanalysis. Electron probe microanalysis was performed using 4 wavelength dispersive spectrometers. Pure Fe and cementite served as reference states for calibration of the carbon signals. The specimens were locked in steel clamps and grinded, polished as for optical microscopy. The tracks to be measured were indicated using micro Vickers imprints. The carbon-concentration profiles were measured with a counting statistical accuracy of 0.04 % C. The 10 keV incident electron beam had a lateral size of about 0.5 μm, which, according to a Monte Carlo simulation for the paths of the electron beams, corresponds to an excited specimen volume of lateral size < 0.8 μm, neglecting the effect of absorption of the emitted CK_α radiation which further reduces the lateral size. The depth of information lies within 0.3 μm (for further details of measurement and evaluation see [19]).

Results and discussion

Choice of the diffusion coefficient of carbon in austenite. *Effect of the initial carbon concentration on the migration rate.* In **figure 3** the ferrite layer thickness is depicted as a function of the initial average carbon concentration, calculated at a temperature of 973 K for a grain size of 25 μm for a transformation time of 5 s. With increasing gross carbon concentration the ferrite layer thickness, and thus the migration rate, decreases. It can be seen that for the higher carbon concentrations the differences between the curves calculated for the three diffusion coefficients are very small. For a low initial carbon concentration the differences between the calculated layer thicknesses increases, with D_3 resulting in the largest layer thickness and D_2 resulting in the smallest layer thickness.

The behaviour as shown in figure 3 can easily be explained. The migration rate of the interface directly depends on the carbon concentration gradient in the austenite ahead of the interface. Therefore, the ferrite layer thickness after a fixed transformation time decreases with increasing initial carbon concentration. Secondly, the effect of the averaging procedure used in determining D_C will be larger for low initial carbon concentrations as the local carbon concentration variations are larger. At high initial carbon concentrations the differences between the three curves become marginal. Since D_2 underestimates the true local diffusion coefficient in the enriched zone ahead of the interface, the ferrite layer thickness calculated for $D_C = D_2$ will always be lower than that calculated for $D_C = D_1$. Similarly D_3 is an overestimate and the ferrite layer thickness calculated will always be slightly too large.

Influence of the carbon concentration at the interface on the migration rate. The other parameter important for the gradient of the carbon concentration near the interface, is the concentration of carbon at the interface itself. For a fixed concentration at the centre of the grain, a higher carbon concentration at the interface leads to a larger gradient. Thus, a higher migration rate is expected. The influence of the carbon concentration in austenite at the interface on the migration rate is shown in **figure 4** for an initial carbon atomic fraction of 0.8 %. An increase of the carbon concentration at the interface leads to an increased migration rate. For a low carbon concentration at the interface the effects of averaging are small and therefore the choice of the diffusion coefficient is not that important. For higher concentrations at the interface, the effects of the choice of the diffusion coefficient become more apparent. The behaviour is comparable, yet inverted to that as shown in figure 3.

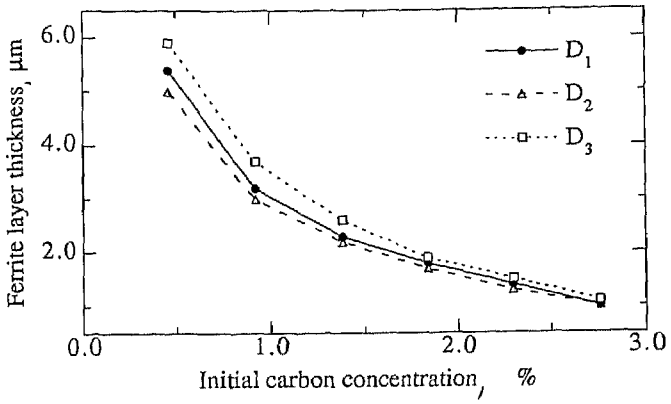

Figure 3. Ferrite layer thickness after 5 s (Δt = 0.1 s) isothermal transformation at a temperature of 973 K as a function of the initial carbon concentration for a grain size of 25 μm (Δx = 0.1 μm)

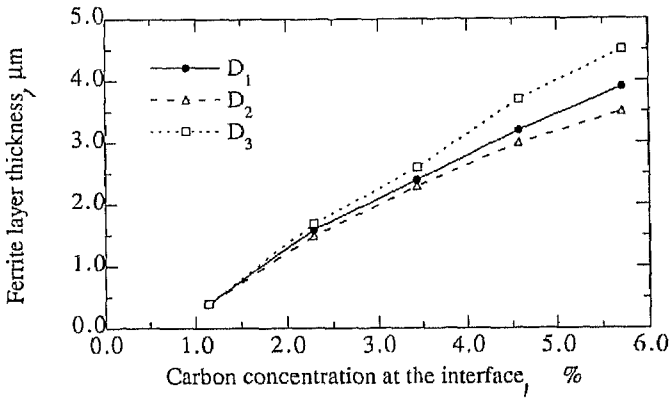

Figure 4. Ferrite layer thickness after 5 s (Δt = 0.1 s) isothermal transformation at a temperature of 973 K as a function of the carbon concentration in austenite at the interface of an Fe 0.8 % C alloy

Complete diffusion controlled growth implies that the carbon concentration at the interface equals the equilibrium concentration at all times. Complete interface controlled growth implies little enrichment at the interface and hence a very small gradient near the interface. Thus, the migration rate as calculated for diffusion controlled growth gives the upper limit for the migration rate and the migration rate as calculated for interface controlled growth gives a lower limit. The model as formulated in this work and in which the carbon concentration alternately decreases from and increases to the equilibrium concentration will provide a migration rate that is somewhere in between both extreme growth controlling processes and implies mixed control of the diffusion of the solute and the processes active at the interface.

Effect of the austenite grain size on the migration rate. A third parameter having an influence on the calculated ferrite layer thickness for different definitions of the diffusion coefficient is the austenite grain size. The ferrite layer thickness in an Fe 0.8 % C alloy after 5 s transformation at 973 K as a function of the austenite grain size is shown in **figure 5**.

From this figure it can be seen that for large grain sizes the ferrite layer thickness does not depend on the grain size

but only on the definition of the diffusion coefficient (the grain resembles a semi-infinite medium). In agreement with results presented in figure 4 the largest ferrite layer thickness is calculated for D_3, and the smallest for D_2. The reduction in the ferrite layer thickness at smaller austenite grain size is due to overlap of the diffusion fields in the centre of the austenite grains. The critical diameter for overlap to occur is 30 μm (D_1 and D_2) or 40 μm (D_3).

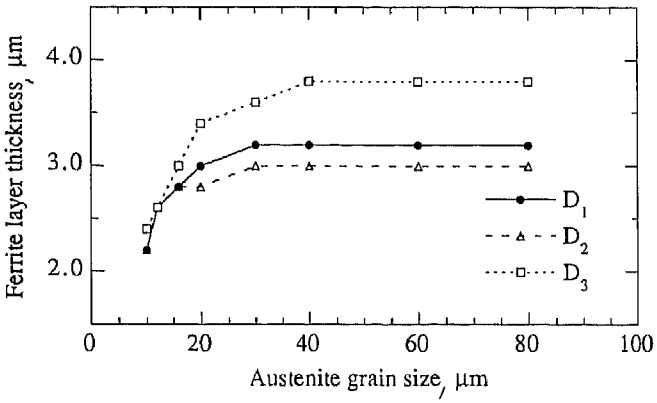

Figure 5. Ferrite layer thickness after 5 s (Δt = 0.1 s) isothermal transformation at a temperature of 973 K as a function the austenite grain size for an Fe 0.8 % C alloy

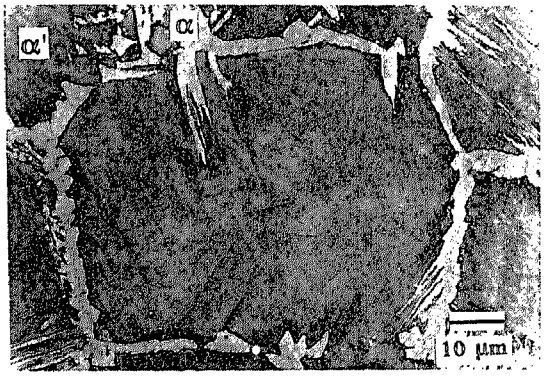

Figure 6. Optical micrograph of an Fe 0.8 % C specimen partially transformed at 973 K for 5 s showing ferrite nucleated at austenite grain boundaries. The length of the scaling bar is 10 μm

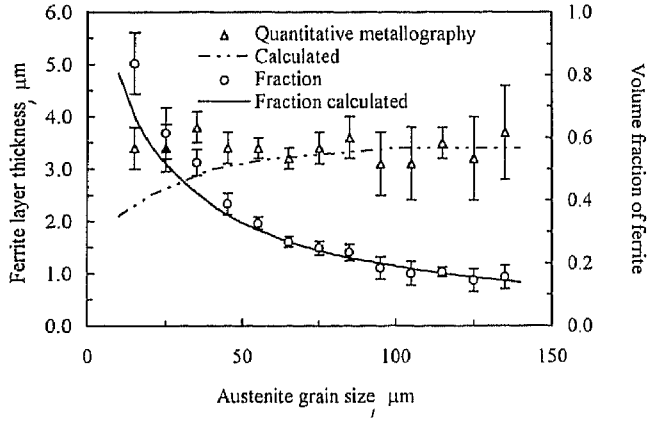

Figure 7. Ferrite layer thickness and the ferrite volume fraction as a function of the austenite grain size as determined from the microstructure of an Fe 0.8 % C alloy, austenitised at 1273 K, partially transformed at 973 K for 5 s, quenched using He-gas. The error bars indicate the standard deviation in the measurement

Determination of the ferrite layer thickness in partially transformed specimens. **Figure 6** shows the microstructure obtained after partial transformation of the Fe 0.8 % C alloy at 973 K for 5 s. The former austenite grain boundaries are completely covered with a layer of ferrite. The morphology of the ferrite formed at the austenite grain boundaries is in fair agreement with the assumptions of nucleation along the entire austenite-grain boundaries and a symmetrical growth of the ferrite. The latter assumption implies that only half of the layer is formed in the grain studied and growth takes place equally fast in two neighbouring grains. This is not completely correct, but, as can be seen from the following pictures, only causes deviations for small grains.

The ferrite layer thickness was determined in several steps. First, the surface area of the former austenite grain was determined, as well as the perimeter of the grain. Then, the surface area of the ferrite was determined and translated into an average ferrite layer thickness. This was performed as a function of the austenite grain size in the Fe 0.8 % C specimen that was partially transformed at 973 K for 5 s. In **figure 7** it can be seen that the ferrite layer thickness is roughly constant for the different grain sizes, in contrast to the theoretical predictions which yield a lower ferrite thickness at smaller austenite grains. However, it should be pointed out that for small austenite grains there is little chance of making a cross-section exactly through the middle of the grain. A slight off-central cross-section yields an overestimate for the ferrite layer thickness. Therefore, in figure 7 the experimental data for small austenite grains will be generally too high. In figure 7 the ferrite volume fraction as a function of the austenite grain size is also shown, using the same set of experimental data.

The progress of the transformation with increasing transformation time is shown in **figure 8** for the Fe 0.8 % C alloy transformed at 973 K. The agreement between experiments and calculations is quite satisfactory. It should be noted however that at the transformation temperature used the formation of Widmanstätten ferrite can also occur. These needle-like ferrite particles grow according to a different mechanism and at a higher rate. The Widmanstätten ferrite can be distinguished from pro-eutectoid ferrite by its morphology, **figure 9**. In the quantitative determination of the total surface area covered by ferrite, no distinction can be made, however, between the Widmanstätten and the pro-eutectoid ferrite. Therefore, the fraction of ferrite determined at later stages might be a slight overestimate of the allotriomorphic ferrite fraction. Yet, the agreement remains quite reasonable.

Measurements of the carbon concentration profiles in partially transformed specimens. The Fe 0.8 % C samples that were isothermally transformed for 5 and 12 s at 973 K were also used to measure the carbon concentration profile across the ferrite/martensite interfaces. The results for a sample isothermally transformed for 5 s are shown in **figure 10**. The experimental ferrite layer thickness of 3-4 μm is in good agreement with the calculated ferrite layer thickness. However, the maximum concentration observed in the vicinity of the interface is significantly below that used in the calculations. This can be explained partially by taking into account the spatial resolution of the EPMA measurements which is significantly lower than the step size used in the calculations. From Monte Carlo simulation experiments it was found that the lateral size of the beam

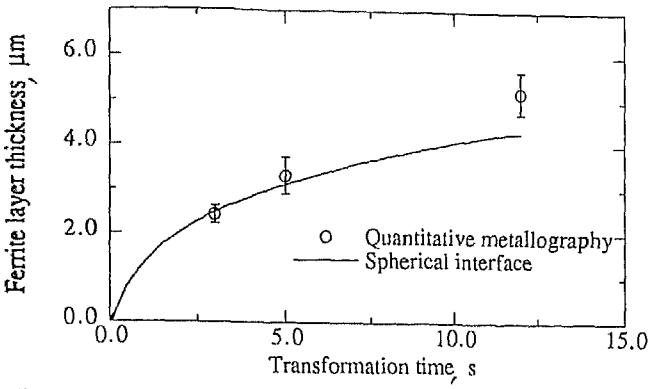

Figure 8. Ferrite layer thickness as a function of the transformation time as determined from the microstructures of an Fe 0.8 % C alloy, austenitised at 1273 K and transformed at 973 K; quenched using He-gas. The calculations were performed for a grain size of 25 μm

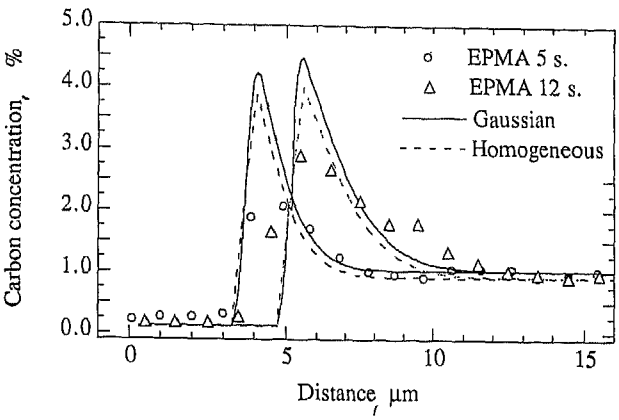

Figure 11. Comparison of the concentration profiles measured experimentally with EPMA in specimens that were isothermally transformed for 5 and 12 s with the profiles calculated (convoluted with a Gaussian intensity distribution function)

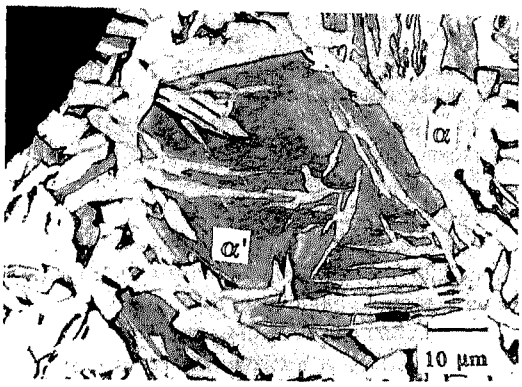

Figure 9. Optical micrograph of an Fe 0.8 % C specimen partially transformed at 973 K for 12 s showing ferrite nucleated at grain boundaries and grown into the austenite grains. Note the increased amount of Widmanstätten ferrite (arrows). The scaling bar is 10 μm

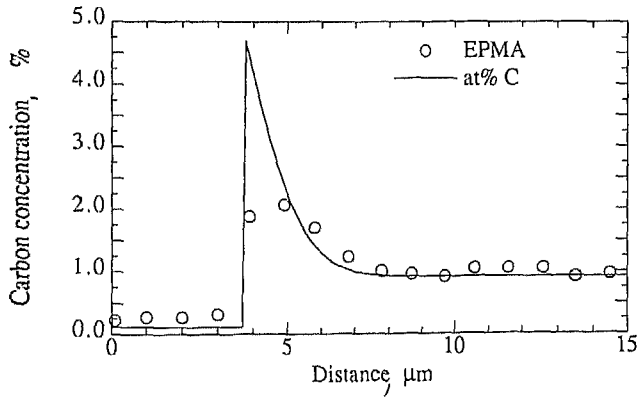

Figure 10. Comparison of the carbon concentration profile determined experimentally in the Fe 0.8 % C specimen after 5 s isothermal transformation at 973 K with the calculated profile

spot was of the order of 0.8-0.9 μm. In order to compare the measured concentration profiles to the calculated profiles, the latter have to be convoluted by some function describing the contribution of each position within the beam spot to the generated X-rays as measured during the analysis. The rather sharp concentration profile is somewhat flattened and the highest concentration in the austenite at the interface would not occur at the interface but at some distance away from the interface. A comparison of the measured data with the calculated concentration profiles convoluted by the an intensity distribution functions now shows a better agreement, **figure 11**, although the maximum carbon concentration still falls significantly below the value used for the calculation.

Comparison of the ferrite growth data to literature data. In literature experimental data on the growth kinetics of ferrite on austenite grain boundaries [14; 20] have been reported before. The data of [20] suffered from severe scatter due to both structural and stereological effects. As a result comparison with numerical models is quite difficult. In [14] the transformation kinetics were followed by measuring the maximum width and maximum length of ferrite particles in partially transformed high-purity Fe-C specimens. Thus the scatter was significantly reduced. These data are commonly used for comparison with diffusion controlled growth models. In [14] the experimental rate constants were smaller than the calculated rate constants for all alloys and for all temperatures investigated. This was attributed to the presence of partially coherent facets at portions of the interface, which reduced the growth rate. The lack of agreement opened the way for further investigation and different models were set up and compared to the experimental data of [14], as in [9; 11]. In [11] growth rates were calculated for different morphologies among which a planar, spherical and also an oblate ellipsoid morphology. Reasonable agreement was achieved for the higher carbon concentrations, yet for the lower concentrations the agreement was less obvious.

In [9] the growth rate of ferrite in Fe-C austenites was modelled assuming site-saturation for nucleation. The growth rate as calculated in [9] was low compared to the lengthening kinetics as measured in [14] and high in comparison to the thickening kinetics of the ferrite. This was explained by attributing the observed differences to processes taking place at highly curved interfaces rather than the smooth interfaces as assumed in the calculations. The effect of an enhanced diffusion rate via the grain boundary was not taken into account. Comparing the results presented in this work to the previous experiments [14] it should be noted that the carbon concentration of the alloy used in this work is somewhat lower than that in [14]. To be able to

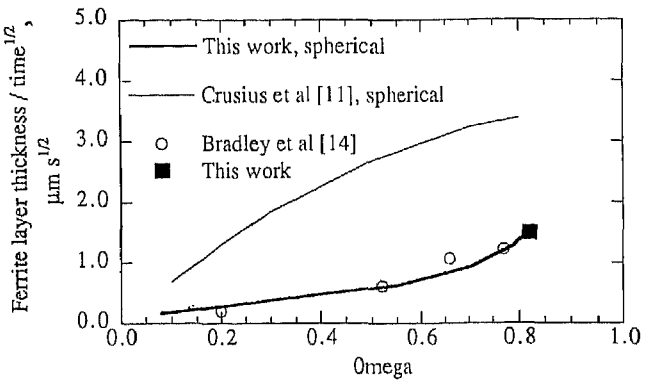

Figure 12. Comparison of experimental (open symbols) and calculated (thin lines) thickening kinetics of allotriomorphic ferrite in austenite from literature to experimental (closed symbol) and calculated data (thick lines) presented in this work as function of supersaturation Ω

compare results, the results are plotted as a function of the supersaturation rather than the temperature. The supersaturation, Ω, is defined as:

$$\Omega = \frac{c^{\gamma/\alpha} - c_C^{\gamma}}{c^{\gamma/\alpha} - c^{\alpha/\gamma}}. \qquad (8)$$

In **figure 12** the parabolic growth rate in an Fe 0.9 % C alloy is shown as a function of the supersaturation for the present model and the present experimental data and for the theoretical [11] and experimental [14] from the literature. Our theoretical results are in good agreement with those of [11] and our experimental data agree well with those of [14]. As in our model the concentration at the interface is, on average, lower than the local equilibrium value imposed in [11] our model results in a lower growth rate which matches the experimental data slightly better. The approach of a variable carbon concentration at the interface has also been demonstrated to be successful for the prediction of the microstructure of iron carbon samples containing vanadium [21], where the driving force for migration is counteracted by a pinning force originating from the precipitation of vanadium carbide. Migration of the interface can only occur if the driving force exceeds the pinning force. While the interface is pinned, the carbon still redistributes within the austenite. As a result the concentration at the interface decreases. Thus the driving force increases, since the chemical potential difference of the Fe atoms across the interface is a function of the carbon concentration in the austenite. The mobility of the interface then is a delicate balance of the (near) interfacial processes, such as precipitation and the diffusion of carbon away from the interface.

In pure Fe-C alloys, a similar reasoning might be applicable even in the absence of precipitation. The volume changes as a result from the transformation going from austenite to ferrite might play a role here. The effect of volume changes is seldom incorporated in diffusion since the volume changes are considered to be rather small [9]. However, since the volume in austenite is a function of the carbon concentration, and the austenite near the interface enriches in carbon the volume changes are locally larger than expected, as is shown in **figure 13** [22]. Austenite containing 0.8 % C, has a volume per Fe atom that is about 1 % smaller than the volume per Fe atom in ferrite. However, austenite with the equilibrium amount of carbon has a volume per Fe atom that is 2-4 % larger than the volume per Fe atom in ferrite in the indicated temperature region. The volume misfit reduces the interface mobility, but not the diffusion rate of carbon. Thus, the carbon redistributes in the austenite thereby decreasing the carbon concentration at the interface. The volume misfit decreases and the driving force for interface migration increases. When the resultant of the driving force and the pinning force becomes positive the interface can migrate again. Reduction of the equilibrium carbon concentration by about 30 % already halves the relative volume difference between austenite and ferrite and can thus significantly reduce volume misfit strains.

The volume misfit can be especially significant at lower temperatures where the volume misfit increases both due an increasing level of enrichment for the equilibrium austenite and by the difference in thermal expansion coefficients between austenite and ferrite.

Conclusions

A numerical model is presented to calculate the interface mobility in Fe-C alloys taking into account the concentration dependence of the diffusion coefficient of carbon in austenite, the austenite grain size and the carbon concentration in austenite at the interface.

- calculated ferrite layer thicknesses are compared for different definitions of the effective diffusion coefficient of carbon in austenite. Significant differences are found for low initial carbon concentration, high carbon concentration at the interface or for large austenite grains;
- the growth of a ferrite layer in austenite normal to the former austenite grain boundaries at tempertures below the A_1 temperature can be accurately described by a diffusion mechanism adopting a time-variant carbon concentration at the interface, where the maximum concentration is prescribed by the local equilibrium model. Thus, a sort of mixed control of diffusion controlled mobility and interface controlled mobility is obtained;

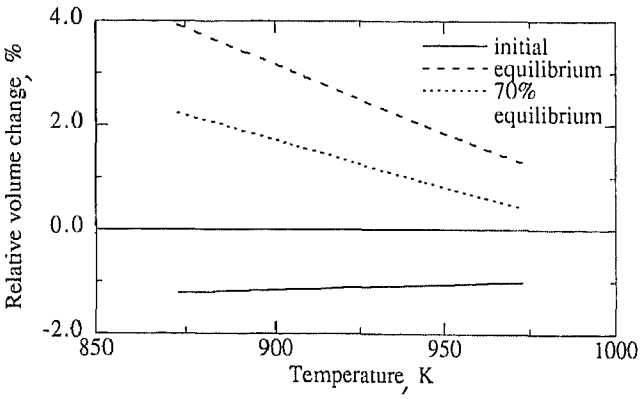

Figure 13. Relative volume changes between ferrite and austenite as function of temperature for various carbon concentrations of austenite. The solid line represents the relative volume difference between the initial (0.8 % C) austenite and ferrite, the large dashed line represents the relative volume difference between austenite according to local equilibrium and ferrite. The small dashed line represents the relative volume difference between austenite and ferrite where the austenite contains an amount of carbon that is 30 % reduced with respect to the equilibrium austenite [22]

- satisfactory agreement between experiments and calculations is achieved. The experimental data on the ferrite layer thickness corresponds to the ferrite layer thickness as calculated assuming mixed control of the interface migration. The convoluted theoretical carbon concentration profiles match the profiles determined experimentally;
- good agreement between theoretical results and both new and existing experimental data was observed.

Acknowledgements

The authors are indebted to Ir. W.G. Sloof for the Electron-Probe Micro Analysis (EPMA) and to Mr. P.F. Colijn for assistance with light microscopy. Financial support by Hoogovens Corporate Research, IJmuiden, The Netherlands, and the Innovative Research Project for Metals of the Dutch government (IOP-Metalen) is gratefully acknowledged.

(A 01 048; received: 17. February 1995;
in revised form: 13. July 1995)

References

[1] *Hawbolt, E. B.; Chau, B.; Brimacombe, J. K.:* Metall. Trans. 16 A (1985), p. 565/78.
[2] *Fernandes, F.; Denis, S.; Simon, A.:* Mem. Et. Sci. Rev. Metall. (1986), p. 335/66.
[3] *Farias, D.; Denis, S.; Simon, A.:* Trait. Therm. 237 (1990), p. 63/70.
[4] *Wilson, E. A.:* Mat. Sci. Techn. 7 (1991), p. 1089/1100.
[5] *Lee, K. J.; Lee, J. K.; Kang, K. B.; Kwon, O.:* ISIJ Intern. 32 (1992), p. 326/34.
[6] *Denis, S.; Farias, D.; Simon, A.:* ISIJ Intern. 32 (1992), p. 316/25.
[7] *Jayaswal, S. K.; Gupta, S. P.:* Z. Metallkde. 83 (1992), p. 809/19.
[8] *Watanabe, T.:* Mat. Res. Soc. Symp. Proc. 122 (1988), p. 443/54.
[9] *Vandermeer, R. A.:* Acta Metall. Mater. 38 (1990), p. 2461/70.
[10] *Enomoto, M.:* ISIJ Intern. 32 (1992), p. 297/305.
[11] *Crusius, S.; Höglund, L.; Knoop, U.; Inden, G.; Ågren, J.:* Z. Metallkde. 83 (1992), p. 729/38.
[12] *Enomoto, M.; Atkinson, C.:* Acta Metall. Mater. 41 (1993), p. 3237/44.
[13] *Kamat, R. G.; Hawbolt, E. B.; Brown, L. C.; Brimacombe, J. K.:* Metall. Trans. 23 A (1992), p. 2469/80.
[14] *Bradley, J. R.; Rigsbee, J. M.; Aaronson, H. I.:* Metall. Trans. 8 A (1977), p. 323/33.
[15] *Crank, J.:* The mathematics of diffusion, Oxford, Clarendon Press, 1970.
[16] *Ågren, J.:* Acta Metall. 30 (1982), p. 841/51.
[17] *Ågren, J.:* Scripta Metall. 20 (1986), p. 1507/10.
[18] *Onink, M.; Brakman, C. M.; Tichelaar, F. D.; Mittemeijer, E. J.; Zwaag, S. van der:* Z. Metallkde., to be published.
[19] *Somers, M. A. J.; Colijn, p. F.; Sloof, W. G.; Mittemeijer, E. J.:* Z. Metallkde. 81 (1990), p. 33.
[20] *Kinsman, K. R.; Eichen, E.; Aaronson, H. I.:* Metall. Trans. 6 A (1975), p. 303/17.
[21] *Liu, W. C.:* Metall. Trans. 24 A (1993), p. 2195/2207.
[22] *Onink, M.; Brakman, C. M.; Tichelaar, F. D.; Mittemeijer, E. J.; Zwaag, S. van der; Root, J. H.; Konyer, N. B.:* Scripta Metall. Mater. 29 (1993), p. 1011/16.